Conflicting evolutionary histories of the mitochondrial and nuclear genomes in New World *Myotis* bats

Roy N. Platt II[1], Brant C. Faircloth[2], Kevin A.M. Sullivan[1], Troy Kieran[3], Travis C. Glenn[3], Michael W. Vandewege[1], Thomas E. Lee[4], Robert J. Baker[1], Richard D. Stevens[5], David A. Ray[1*]

[1] Department of Biological Sciences, Texas Tech University, Lubbock, USA

[2] Department of Biological Sciences and Museum of Natural Science, Louisiana State University, Baton Rouge, USA

[3] Environmental Health Science, University of Georgia, Athens, USA

[4] Department of Biology, Abilene Christian University, Abilene, USA

[5] Natural Resource Management, Texas Tech University, Lubbock, USA

*Corresponding author: E-mail: david.4.ray@gmail.com

Abstract

The rapid diversification of *Myotis* bats into more than 100 species is one of the most extensive mammalian radiations available for study. Efforts to understand relationships within *Myotis* have primarily utilized mitochondrial markers and trees inferred from nuclear markers lacked resolution. Our current understanding of relationships within *Myotis* is therefore biased towards a set of phylogenetic markers that may not reflect the history of the nuclear genome. To resolve this, we sequenced the full mitochondrial genomes of 37 representative *Myotis*, primarily from the New World, in conjunction with targeted sequencing of 3,648 ultraconserved elements (UCEs). We inferred the phylogeny and explored the effects of concatenation and summary phylogenetic methods, as well as combinations of markers based on informativeness or levels of missing data, on our results. Of the 294 phylogenies generated from the nuclear UCE data, all are significantly different from phylogenies inferred using mitochondrial genomes. Even within the nuclear data, quartet frequencies indicate that around half of all UCE loci conflict with the estimated species tree. Several factors can drive such conflict, including incomplete lineage sorting, introgressive hybridization, or even phylogenetic error. Despite the degree of discordance between nuclear UCE loci and the mitochondrial genome and among UCE loci themselves, the most common nuclear topology is recovered in one quarter of all analyses with strong nodal support. Based on these results, we re-examine the evolutionary history of *Myotis* to better understand the phenomena driving their unique nuclear, mitochondrial, and biogeographic histories.

Keywords

summary tree methods, concatenation, Vespertilionidae, phylogenomics, UCE, ultraconserved elements, reticulation, incomplete lineage sorting

38 The bat genus *Myotis* (Order Chiroptera, Family Vespertilionidae) comprises more than 100
39 species that originated during the last 10-15 million years (Stadelmann et al. 2007), making it one of the
40 most successful, extant, mammalian radiations. *Myotis* are distributed worldwide, excluding polar
41 regions, and generally share a similar ecological niche: aerial insectivory. *Myotis* species often exhibit
42 little morphological differentiation and, as a result, the rate of cryptic speciation within the genus is
43 thought to be high. For example, specimens identified as *M. nigricans* and *M. albescens* form multiple
44 paraphyletic lineages distributed throughout the phylogeny of Neotropical *Myotis* (Larsen et al. 2012).
45 Confounding matters, the morphological variation that exists is often a poor indicator of species-level
46 relationships. Early classifications of *Myotis* identified three major morphotypes (Findley 1972).
47 Subsequent phylogenetic analyses of the mitochondrial cytochrome-b (*cytb*) gene demonstrated
48 paraphyletic origins of each morphotype, suggesting frequent convergent evolution (Ruedi et al. 2001).
49 These same analyses demonstrated that geography was a better predictor of phylogenetic relationship
50 than morphology (Ruedi et al. 2001, Stadelmann et al. 2007).
51 The ability of mitochondrial markers to resolve a well-supported topology does not guarantee
52 that the mitochondrial tree represents the species tree (for examples see Willis et al. 2014, Li, Gang et
53 al. 2016, Leavitt et al. 2017). The lack of recombination and uniparental inheritance of the
54 mitochondrion means that it is transmitted as a single genetic unit that is susceptible to evolutionary
55 processes that may cause its history to diverge from the history of the species (Edwards et al. 2009). The
56 most widely accepted phylogenies of *Myotis* rely heavily on mitochondrial data and even phylogenies
57 containing nuclear data demonstrate an over reliance on mitochondrial markers for resolution, likely
58 swamping out potentially conflicting signals from the nuclear genome. For example alignments of the
59 nuclear *RAG*2 and mitochondrial *cytb* contained 162 and 560 variable characters, respectively
60 (Stadelmann et al. 2007). Despite these concerns, we find ourselves in a situation where our
61 understanding of evolutionary relationships, our basis for conservation strategies, and our
62 biogeographic hypotheses are all founded, almost entirely, on mitochondrial phylogenies.
63 Targeted sequencing of ultraconserved elements (UCEs; Faircloth et al. 2012) to collect
64 sequence data from thousands of loci across the nuclear genome has resolved a number of difficult
65 phylogenetic problems (for examples see Faircloth et al. 2012, McCormack et al. 2013, Green et al. 2014,
66 Faircloth et al. 2015, McGee et al. 2016). Here we used UCE baits to collect ~1.4 Mbp from ≥3,600
67 nuclear loci in addition to random shotgun sequencing to collect full mitochondrial genomes in 37 taxa,
68 primarily representing New World (NW) *Myotis*. Rather than analyzing each sequence data set once, or
69 a handful of times, we chose to use a range of sampling, partitioning, and inference methods to fully

70 explore phylogenetic tree space of the nuclear and mitochondrial genomes. We recovered 294 trees
71 representing 175 distinct topologies for the nuclear UCE data and 28 trees representing 14 distinct
72 mitochondrial topologies. Our results show that, despite the range of trees recovered from each marker
73 type, nuclear and mitochondrial markers occupy distinct regions in tree space. Given that the nuclear
74 and mitochondrial trees are distinct from one another it is necessary to reevaluate hypotheses made
75 based solely on the mitochondrial phylogeny.
76
77 **RESULTS**
78 We used targeted sequencing of UCEs in 37 individuals (Table 1) to collect sequence data from
79 3,648 nuclear loci which we assembled into concatenated alignments as large as 1.37 Mb. In addition,
80 we assembled mitochondrial genomes for most taxa from random shotgun sequencing data. We then
81 used the data to infer the phylogenetic history of New World *Myotis* using a range of locus sampling
82 strategies, alignment partitioning methods and phylogenetic inference methods.
83 *Mitochondrial assembly, alignment, and phylogenetic inference*
84 We generated an average of 5,498,440 paired reads per sample (min = 2,2370,68, max =
85 9,961,348) reads per sample of random DNA sequence data for mitochondrial genome assembly.
86 Assemblies varied in quality. Some were almost entirely complete while others were missing small
87 regions. We were not able to assemble through the control region for any of the samples. We found
88 three premature stop codons in mtDNA protein coding genes. Subsequent manual alignment and
89 validation suggested that these regions were miscalled by MitoBim, and we corrected the errors prior to
90 analysis. Sequence coverage of the mitochondrial genomes averaged 58x (range >1x - 297x).
91 The thirty-seven mitochondrial protein coding, rRNA and tRNA genes were concatenated into an
92 alignment of 15,520 bp containing 5,007 informative characters. rRNA and tRNA genes were
93 concatenated into an alignment containing 4,157 bp containing 862 parsimony informative characters.
94 Protein coding genes were concatenated into an alignment containing 11,363 bp or 3770 amino acids
95 (aa) and containing 4,145 or 509 parsimony informative characters, respectively. For the alignment
96 containing all protein coding, rRNA and tRNA genes, 30 samples were ≥ 90% complete, and alignments
97 for five samples were 68-84% complete. Only 21% and 50% of nucleotide positions were present in the
98 *M. albescens*[3] (TK 61766) and *M. levis* alignments, respectively.
99 When considering alignment type, partitioning strategy, and phylogenetic inference method we
100 analyzed the mitochondrial data 28 ways as described in the Methods. These analyses recovered 14
101 distinct topologies, the most common of which was recovered 6 times, all by analysis of the translated

102 protein coding genes (Figure 1A). Despite being the most common topology, bipartition frequencies and
103 clade probability values were lower than nucleotide based datasets, as would be expected with more
104 slowly evolving amino acid sequences. Analysis of RNA coding genes recovered two topologies
105 depending on the method of phylogenetic inference. The remainder of the analyses recovered various
106 trees without any pattern relating to partitioning scheme or inference method. A majority rule
107 consensus tree for all 28 analyses is shown in Figure 1C. The mitochondrial consensus tree reflects
108 previously reported mitochondrial phylogenies for *Myotis*. The New World *Myotis* are generally
109 monophyletic splitting into Nearctic and Neotropical clades with the Old World taxon, *M. brandtii*, sister
110 to the Neotropical clade. Ambiguity, represented by polytomies, is found only in terminal relationships.

111 *UCE assembly and alignment, and phylogenetic inference*

112 We averaged 3.29 million reads per sample after demultiplexing reads from the UCE-enriched,
113 sequencing pool. These reads were assembled into an average of 5,778 contigs per sample (min = 1,562
114 *M. nyctor*, max = 11,784 *M. nigricans* [3]). Recovery rates for UCE loci varied across taxa. Of the 5,500 loci
115 in the Amniote probe set, we successfully recovered 3,898 UCE loci, 3,648 loci from five or more
116 samples and 212 loci in all 37 samples (Table 2). On average, 3,332 UCE loci were recovered per sample,
117 ranging from 1,106 (*M. nyctor*) to 4,008 (*M. keaysi*). Repetitive sequences, identified via RepeatMasker
118 searches, were minimal, occupying less than 0.02% of sites across all UCE alignments.

119 In all, 294 different combinations of alignment, partitioning, and inference method were used to
120 identify 175 unique nuclear topologies. The most common tree was recovered 45 times (Figure 1B). All
121 nodes were highly-supported based on clade probability values and all but three nodes were highly
122 supported with maximum likelihood bootstrap replicates. A consensus tree (Figure 1D) of the 294
123 nuclear topologies resolves New World *Myotis* (and *M. brandtii*) as a single polytomy that excludes *M.*
124 *volans* and represents a departure from previous mitochondrial phylogenies, including the one
125 recovered herein. Comparison of the mitochondrial and nuclear consensus trees (Figures 1C and D)
126 reveals substantial differences in the relationships within the genus.

127 As noted above, we were concerned that phylogenetic error, sampling bias or other factors may
128 be driving the conflict between the mitochondrial and nuclear trees. We started by investigating the
129 effects of matrix composition (or completeness) on phylogenetic inference using UCE loci by generating
130 10 alignments having varying levels of matrix completeness. Nine alignments were composed of loci
131 with 15 to 95% (at 10% intervals) of taxa. The tenth alignment was composed of all loci which were
132 recovered in 100% of specimens examined. For example, in the '15%' matrix, all loci that were
133 represented in at least 15% of species ($n_{taxa} \geq 5$) were included in the alignment (n_{loci} = 3,648). In the

134 '100%' matrix, only loci which were identified in all species (n_{taxa} = 37) were included (n_{loci} = 212).
135 Alignments were partitioned using three schemes: unpartitioned, individually partitioned by locus, or
136 combined partitions. Alignment lengths, numbers of informative characters and number of partitions
137 identified by PartitionFinder are available in Table 2. The result was 10 alignments that were each
138 partitioned three ways. These were analyzed with Bayesian, maximum likelihood, and coalescent
139 methods using RaxML, ExaBayes, ASTRID, ASTRAL-II and SVDquartets as described in the Methods.
140 Bootstrap topologies stabilized in each alignment and partition combination within 150 replicates and all
141 Bayesian runs converged in less than ten thousand generations. Unfortunately, computational limits
142 forced us to abandon the individually partitioned, Bayesian analyses. In general, the same alignment
143 produced the same topology regardless of inference method or partitioning scheme with the only
144 exception being the terminal relationships of the *M. levis*/*M. albescens* clade in the combined vs.
145 unpartitioned Bayesian analysis of the 100% complete data matrix.

146 Trees were also generated from data matrices incorporating UCE loci of differing lengths
147 (Hosner et al. 2016). All 3,648 loci were grouped into ten bins based on locus length so that the first bin
148 contained the 365 shortest loci, the second bin contained the 366th to the 731st, and so on. The number
149 of informative characters per bin ranged from 1,115 to 6,995 and the number of informative characters
150 was correlated with average locus length (Supplemental Figure 1). On average, only 2.6% of characters
151 in each bin were parsimony-informative (Supplemental Figure 1). Each of the ten length-based
152 alignments recovered slightly different topologies. Terminal relationships were generally stable across
153 analyses with the majority of differences between topologies found in the early bifurcations of the
154 ingroup (*Myotis*).

155 From the above results, we observed that, in general, longer alignments produced well resolved
156 topologies with significant nodal support regardless of the phylogenetic method or partitioning scheme
157 used. Analyses of smaller data sets were more likely to recover unique topologies.

158 Given the goal of fully exploring nuclear tree space and generating as many reasonable nuclear
159 UCE based topologies for comparison with the mitochondrial tree, we decided to randomly sample a
160 limited number of nuclear UCE loci to create small alignments that would be more likely to result in
161 unique topologies. We therefore randomly subsampled UCE loci to create 100 unique data sets of 365
162 loci. Loci were concatenated in each replicate data set and analyzed using maximum likelihood in
163 RAxML. Of the 100 alignments analyzed, 80 unique topologies were generated (mean Robinson-Foulds
164 distance = 4.3).

165 In addition to concatenation methods we explored phylogenetic tree space of the UCE data set
166 using species tree methods. Normalized quartet scores from ASTRAL-II (Mirarab et al. 2015) analyses
167 were consistent among all analyses, with scores ranging from 0.540 to 0.553, and the number of
168 induced quartet gene trees ranging from 7,745,739 (100% complete 212 gene trees) and 63,042,410
169 (15% 3648 loci). SVDquartets (Chifman et al. 2014) sampled all 66,045 quartets. On average, the total
170 weight of incompatible quartets was 2.84%. Similar to the concatenated analysis, we inferred
171 coalescent-based species from the same 100 subsamples of 365 loci described above. Despite being
172 generated from the same underlying data, summary and concatenation methods only recovered the
173 same tree in 1 of 100 attempts.
174 Finally, we used weighted and unweighted statistical binning to combine individual gene trees
175 into supergenes, estimate the supergene phylogeny, and then infer the species tree from the supergene
176 trees. The 3,648 loci were combined into 528 binned loci with 480 bins containing seven loci each and
177 48 bins containing six loci each. Binning methods increases the normalized quartet scores from an
178 average of 0.547 with gene trees to 0.672 for the binned-unweighted and 0.673 for the binned-weighted
179 supergene trees. Given the relatively even distribution of loci into bins the negligible difference in
180 quartet/species tree discordance between the unweighted and weighted supergene trees is expected.
181 Binning methods have been shown to recover incorrect species trees under coalescent methods by
182 altering gene tree frequencies. In addition, it is possible that support for incorrect trees can actually
183 increase with the number of input gene trees (Liu et al. 2015). With these concerns in mind, both
184 binning methods recovered the same topology which was the most common nuclear topology observed
185 across all analyses (Figure 1C).
186 *Topological comparisons*
187 All mitochondrial and nuclear trees are available in Supplemental File 1. When visualizing all
188 topologies in tree space, nuclear trees co-localized and were distinct from mitochondrial topologies
189 (Figure 2A). Comparisons of Robinson-Foulds symmetrical differences show 26 symmetrical differences
190 between the most similar nuclear and mitochondrial trees (Figure 2B). For comparison only 9 of 43,070
191 and 0 of 378 pairwise nuclear vs. nuclear and mitochondrial vs. mitochondrial tree comparisons, Figures
192 2C and D, respectively, exhibited more than 26 symmetrical differences.
193 Of the 45 analyses that recovered the most frequently observed topology (Figure 1D), 38 were
194 Bayesian and RAxML searches that varied by matrix completeness and partitioning scheme. The fact that
195 these analyses recovered the same topology is expected given that they are not independent. For
196 example, a RAxML analysis of the 25% complete data set uses 1.26 Mb of the 1.38 Mb of data present in

197 the 15% complete matrix, sharing 91% of the data. Analyses that directly varied the alignments and/or
198 sampled less data (e.g. randomly sampling loci) were more likely to generate unique topologies than the
199 nested analyses described above. Of the 200 analyses that randomly sampled UCE loci 164 unique
200 topologies were observed. This implies that when analyses of large data sets produce well-resolved
201 trees with significant nodal support, sampling smaller portions of the data, may provide a mechanism
202 for creating phylogenetic uncertainty not represented by typical tree scoring metrics.
203
204 **DISCUSSION**
205 We analyzed 3,648 UCE loci and mitochondrial genomes of 37 *Myotis* bats and outgroups. The
206 mitochondrial and nuclear UCE phylogenies recovered distinct topologies (Figure 1), whether comparing
207 the most commonly recovered or consensus topologies. Previous work with UCE loci demonstrated that
208 support for deep divergences varied based on the number of loci examined (McCormack et al. 2013).
209 Further, bootstrap replicates and clade probability values can be inaccurate metrics of nodal support
210 (Douady et al. 2003, Hedtke et al. 2006). We used varied the input data and phylogenetic parameters to
211 produce a range of reasonable nuclear and mitochondrial topologies that may be more useful than
212 overreliance on a tree resulting from a one or two analyses. Rather than rejecting concordance between
213 the two data types from a single analysis we took steps to analyze both data sets to generate as many
214 viable topologies as possible, possibly revealing hidden overlap between marker types that are masked
215 by phylogenetic error.
216 We recovered 175 and 14 unique nuclear and mitochondrial topologies from 294 and 28
217 analyses using multiple methodologies, sampling strategies, and phylogenetic parameters. By varying
218 our phylogenetic methods we show that recovering a consistent topology is difficult even when using
219 the same marker type, thus making it difficult to determine the "best" topology. Rather than choosing
220 single trees to represent the nuclear and mitochondrial data, we use consensus trees to represent the
221 ambiguity that is present through all analyses along with example phylogenies conforming to the most
222 common topology (Figure 1). Despite our efforts to identify as many plausible, distinct nuclear and
223 mitochondrial trees as possible we were unable recover overlapping topologies between marker types
224 suggesting that nuclear UCE loci and the mitochondrial genomes of *Myotis* have distinct evolutionary
225 histories.
226 A comparison of topologies in tree space illustrates the differenced in trees generated for each
227 data set (Figure 2A). Intra-marker discordance, as measured by differences in nuclear vs. nuclear or
228 mitochondrial vs. mitochondrial topologies is low. Pairwise comparisons of nuclear topologies contain

229 an average of 8.3 symmetrical differences, mitochondrial comparisons contain an average of 10.8
230 differences. By contrast, pairwise differences between nuclear and mitochondrial topologies contain an
231 average of 33.3 symmetrical differences. The two most similar nuclear and mitochondrial topologies
232 contain 26 symmetrical differences. Of the 43,072 pairwise comparisons of nuclear topologies, only 27
233 contain more than 26 symmetrical differences. Likewise of the 378 pairwise comparisons of
234 mitochondrial topologies only 1 contains more than 26 symmetrical differences. These observations
235 indicate that discordance between marker types (Figure 2B) is much greater than within marker type
236 (Figure 2C and 2D). All but the most divergent nuclear topologies are more similar to each other than
237 any nuclear vs. mitochondrial comparison.

238 Conflict between mitochondrial and nuclear data may be driven by error in phylogenetic
239 estimation or may reflect genuine discordance between the two marker types (Degnan et al. 2009,
240 Huang, Huateng et al. 2010). We relied on multiple tree-inference methods (e.g. summary vs.
241 concatenation), manipulated phylogenetic parameters (e.g. partitioning strategy), and sampling criteria
242 (e.g. loci sampled in all taxa) to minimize the impacts of phylogenetic error on the data sets. In most
243 cases, varying parameters or methodologies generated unique topologies with minor differences. In
244 most cases unique topologies resulted from rearrangements of a few terminal taxa. For example,
245 placement of *M. volans* and *M. brandtii* was often either sister to the remaining New World *Myotis* or as
246 an early bifurcation between the Nearctic and Neotropical clades. *M. vivesi* was at times found as sister
247 to the clade containing *M. lucifugus*, *occultus* and *fortidens* or as sister to the clade containing the
248 neotropical *Myotis*.

249 Summary methods failed to recover the most common nuclear topology (Figure 1D) except
250 when loci were binned prior to gene tree estimation. Summary methods also tended to recover more
251 unique topologies than concatenation methods when analyzing data from the same gene(s). For
252 example, the random sample analyses recovered 80 unique topologies using concatenation (RAxML) and
253 89 unique topologies with summary methods (ASTRAL-II). This likely has to do with the limited number
254 of informative characters per locus and by extension limited phylogenetic signal per gene tree
255 (Supplemental Figure 1). In these instances, limited phylogenetic signal per gene would likely lead to
256 increased opportunity for phylogenetic error in gene tree estimation. Further supporting this idea,
257 binning of compatible UCE loci may have indirectly increased phylogenetic signal resulting in the same
258 topology that many of the concatenation analyses recovered. No other summary/coalescent method
259 recovered this topology.

260 Previous studies that used primarily mitochondrial data recovered effectively the same
261 relationships among *Myotis* as our mitochondrial analyses (Ruedi et al. 2001, Stadelmann et al. 2007,
262 Roehrs et al. 2010, Larsen et al. 2012, Ruedi et al. 2013, Haynie et al. 2016). Thus, we are confident that
263 the mitochondrial phylogeny we recovered here, and by others, reflects the true mitochondrial tree.
264 However, the mitochondrial topology may not adequately reflect the species history, particularly when
265 considering the factors that cause incongruence between nuclear and mitochondrial gene trees. Causes
266 of conflicting gene trees include horizontal transfer, gene duplication, introgressive hybridization, and
267 incomplete lineage sorting. The rapid radiation of this clade as well as other biological factors suggests
268 that some of these phenomena are more likely to have influenced the *Myotis* radiation than others.
269 Horizontal transfer of genes is thought to be rare in eukaryotes, but, vespertilionids in general
270 (Thomas et al. 2011, Platt et al. 2014, Platt et al. 2016), and *Myotis* in particular (Pritham et al. 2007, Ray
271 et al. 2007, Ray et al. 2008, Pagan et al. 2010), have experienced horizontal transfer of DNA transposons.
272 These events would not be reflected in our phylogeny because repetitive sequences were removed prior
273 to phylogenetic analyses. More generally, gene duplications could create conflicting signal among
274 individual UCE markers (ex. comparing non-orthologous UCE loci), but the number of gene duplication
275 events would have to be very high to impact enough of the 3,648 UCE loci to confound the
276 mitochondrial and nuclear phylogenies. Further ruling out gene duplication events as the dominant
277 cause of conflicting phylogenetic signal is the fact that such events are likely depressed in *Myotis* as
278 evidenced by their smaller genome size (~2.2 Gb) and trend towards DNA loss (Kapusta et al. 2017)
279 combined with low rates of paralogy in UCEs general (Derti et al. 2006).
280 Introgressive hybridization and reticulation could significantly influence the phylogenies of
281 *Myotis* in a way that leads to conflicting signal between the nuclear and mitochondrial genomes (Sota
282 2002, Good et al. 2015). Hybridization in bats may be relatively common given their propensity to
283 swarm at cave entrances for breeding purposes. In European *Myotis*, swarming has allowed for high
284 degrees of hybridization between *M. brandtii, M. mystacinus, and M. alcathoe* (Bogdanowicz et al.
285 2012). Further, *M. evotis*, *thysanodes*, and *keeni* all experienced historical gene flow during their
286 divergence (Carstens et al. 2010, Morales et al. 2016). We could also explain the differences between
287 the mitochondrial and nuclear UCE phylogenies if *Myotis* experienced extensive incomplete lineage
288 sorting during their radiation. Two factors influence the rate of lineage sorting, the fixation rate and the
289 speciation rate (Hudson et al. 2002). Increasing the time to fixation and/or decreasing the amount of
290 time between cladogenic events will increase the likelihood of incomplete lineage sorting. *Myotis* are
291 generally long lived species (Dzeverin 2008) and underwent a rapid radiation between 5-10 MYA (Lack et

292 al. 2010), suggesting that *Myotis* species are likely to experience higher levels of lineage sorting. The
293 importance of these events - introgressive hybridization and incomplete lineage sorting - in driving the
294 differences between the mitochondrial and nuclear phylogenies should be further explored.

295 *Evolutionary history of* Myotis

296 Our understanding of relationships within *Myotis* is heavily biased by mitochondrial data
297 because nuclear markers were harder to collect and produced fewer informative sites (Ruedi et al. 2001,
298 Stadelmann et al. 2007, Lack et al. 2010, Roehrs et al. 2010, Larsen et al. 2012, Ruedi et al. 2013, Haynie
299 et al. 2016) or nuclear phylogenies with large numbers of makers contained limited numbers of taxa
300 (Platt et al. 2015). Our UCE-based results indicate that nuclear trees vary substantially from the
301 mitochondrial tree. Given that the nuclear and mitochondrial trees are different, we find it necessary to
302 re-evaluate *Myotis* in the context of the nuclear data.

303 Paraphyly of *M. nigricans* and *M. albescens* was inferred from previous mitochondrial
304 phylogenies. Larsen et al. (2012) identified a minimum of four and potentially twelve lineages in *M.*
305 *albescens* and *M. nigricans*. Our sampling included three *M. albescens* and two *M. nigricans*, compared
306 to Larsen's 17 and 29 samples. Despite different mitochondrial and nuclear topologies overall, our
307 mitochondrial and nuclear phylogeny recovered the same paraphyletic clade of three *M. albescens*
308 samples and *M. levis*. Close relationships between these taxa was found in previous work and is
309 expected. More importantly we did not find that *M. albescens* was paraphyletic across much of
310 neotropical *Myotis*. We also found that *M. nigricans* is monphlyletic in the nuclear tree, but paraphyletic
311 in the mitochondrial tree. These results from *M. nigricans* and *M. albescens* are interesting but further
312 inference is limited due to low sample sizes for these taxa.

313 The original subgeneric taxonomy of *Myotis* was based on three morphotypes that were later
314 shown to be the result of convergent evolution (Ruedi et al. 2001). If lineage-sorting affected the
315 mitochondrial phylogeny, it is possible that the morphotypes truly are monophyletic. However,
316 superimposing the previous subgeneric/morphological classification onto the species tree shows an
317 interspersed distribution of morphotypes throughout the most common and consensus nuclear
318 topologies (Figures 1A and B). Many strongly supported terminal relationships link species with different
319 morphotypes. Based on these results, it appears that the three major morphotypes in *Myotis* are indeed
320 a result of convergent evolution, as suggested by previous work (Ruedi et al. 2001, Stadelmann et al.
321 2007) despite the conflicting mitochondrial and nuclear phylogenies recovered

322 Among the more dramatic differences between the nuclear and mitochondrial topologies is the
323 placement of *M. volans* and *M. brandtii* as sister to all New World taxa by the nuclear data. Our

mitochondrial analyses place *M. volans* within a Nearctic clade and *M. brandtii* directly in-between the Nearctic and Neotropical bifurcations (Figure 1A and C) as has been previously reported (Stadelmann et al. 2007). By contrast the consensus UCE tree (Figure 1D) places *M. brandtii*, a species distributed throughout the Old World, within a polytomy at the base of the New World *Myotis* radiation and *M. volans* sister to all New World *Myotis* (including *M. brandtii*). The placement of *M. brandtii* in the nuclear UCE consensus tree does not necessarily contradict the mitochondrial phylogeny since it is an unresolved polytomy. However, it is worth noting that the most commonly recovered nuclear topology (Figure 1B) places *M. brandtii* sister to all New World *Myotis* (excluding *M. volans*). This relationship would more closely affiliate *M. brandtii* with other Old World taxa. The placement of *M. volans* as sister to all New World taxa (including *M. brandtii*) in the most common nuclear tree is a significant departure from previous work and, at first glance, does not make as much sense in a biogeographic framework. *M. volans* is distributed across western and northwestern North America as far as far north as Alaska. *M. brandtii* is distributed across much of Northern Europe and into the extreme eastern regions of Siberia. The key may lie in understanding the biogeography and phylogenetics of a third species, *M. gracili*s, a species that we were unfortunately unable to include.

M. gracilis, along with *M. brandtii*, are the only two *Myotis* geographically distributed in the Old World, but phylogenetically affiliated with the New World *Myotis* (Stadelmann et al. 2007). If future work verifies the sister relationship between *M. brandtii* and *M. gracilis*, then we can envision a scenario where *M. gracilis, M. brandtii,* and *M. volans* are the result of cladegenic events that occurred during the transition of *Myotis* from the Old World to the New World. It is important to remember that this interpretation relies on a fairly dramatic departure from the currently accepted mitochondrial relationships of *M. volans* (represented here by a single sample) to other *Myotis* species and abandons the nuclear UCE consensus tree for the most frequently recovered UCE topology. In addition, our taxonomic sampling excludes *Myotis* species from the OW, Ethiopian clade, the sister clade to New World *Myotis* (Ruedi et al. 2001, Stadelmann et al. 2007, Lack et al. 2010, Ruedi et al. 2013). Taxa from the Ethiopian clade are needed to properly root the New World *Myotis* clade and understand its biogeographic origins. With these caveats in mind, the hypothesis presented here should be viewed as highly speculative. Increasing the number of *Myotis* lineages sampled will shed additional light on this hypothesis.

Other taxa with conflicting positions between marker types include *M. lucifugus* + *M. occultus*, *M. fortidens*, and *M. vivesi*. In general, these relationships are characterized by very short branches (Figure 1D) and are the most likely to be affected by incomplete lineage sorting or limited phylogenetic

356 information. This could explain the strong support with the mitochondrial tree compared to the nuclear
357 species tree, while allowing for a number of nuclear loci to disagree with the species tree, as well.
358 There are a number of monophyletic groups identified with nuclear data (Figure 1A) that share
359 general morphologies. For example, all of the long-eared bats (*septentrionalis*, *auriculus*, *evotis*,
360 *thysanodes* and *keenii*) represent a monophyletic group of higher elevation, forest-dwelling species that
361 glean insects off of surfaces (Fitch et al. 1979, O'Farrell et al. 1980, Warner 1982, Manning et al. 1989,
362 Caceres et al. 2000). The group represented by *fortidens*, *lucifugus* and *occultus* represent a relatively
363 long-haired form of *Myotis*. While having a distinct dental formula, *fortidens* was historically described
364 as a subspecies of M. *lucifugus* (Miller Jr et al. 1928) and *occultus* has alternately represented its own
365 species or been considered a subspecies of *lucifugus* (Hollister 1909, Valdez et al. 1999, Piaggio et al.
366 2002). The clade consisting of *keaysi*, *oxyotus*, *ruber*, *riparius*, and *diminutus* represents a neotropical
367 group of primarily woolly-haired bats (LaVal 1973). None of these relationships are monophyletic in the
368 consensus or most common mitochondrial topologies. If the mitochondrial genome has been subjected
369 to phenomena that obscure the true species tree then these species groups, along with their
370 synapomorphic morphological features, can be reevaluated.
371 *Conclusions*
372 Relationships within *Myotis*, which until now have relied heavily on mitochondrial data, served
373 as the basis for species identification (Puechmaille et al. 2012), evolutionary hypotheses (Simões et al.
374 2007), and even conservation recommendations (Boyles et al. 2007). Previous studies using nuclear data
375 have largely been uninformative or utilized too few samples to draw definitive conclusions. Trees
376 estimated from ~3,650 nuclear loci and 295 phylogenetic analyses recovered 175 topologies, none of
377 which are congruent with the mitochondrial phylogeny of *Myotis*. Conflict between the mitochondrial
378 and nuclear trees as well as among individual nuclear loci suggest that the *Myotis* radiation may have
379 been accompanied by high levels of incomplete lineage sorting and possible hybridization. Rather than
380 placing emphasis on the mitochondrial tree, it may be more appropriate to consider it for what it really
381 is: a single gene on par with a single UCE locus, albeit one with many more phylogenetically informative
382 characters. If true, then the mitochondrial genome is as likely to reflect the true species tree as any
383 single UCE locus chosen at random. Phenomena such as lineage sorting, reticulation, and introgression
384 have likely influenced the genomes of *Myotis* and should be accounted for in subsequent work. It is
385 possible that the *Myotis* radiation is more accurately reflected as a hard polytomy or a phylogenetic
386 network rather than a strictly bifurcating phylogeny.
387

388 **MATERIALS AND METHODS:**

389 *Taxon Selection*

390 Taxa were selected to span the major phylogenetic break points with emphasis on the Nearctic
391 and Neotropical bifurcation as recovered in previous mitochondrial phylogenies (Stadelmann et al. 2007,
392 Ruedi et al. 2013). In addition, multiple individuals morphologically identified as *M. nigricans* and *M.*
393 *albescens* were included to test for paraphyly as suggested by Larsen et al. (2012). Three Old World
394 species of *Myotis* and the outgroup, *E. fuscus,* were included to root phylogenetic analyses. All field
395 identifications were confirmed from voucher museum specimens. Information for all specimens
396 examined is available in Table 1.

397 *Library preparation, sequencing, and processing*

398 Genomic DNA was extracted from 33 samples using either a Qiagen DNEasy extraction kit or a
399 phenol-chloroform/ethanol precipitation. DNA was fragmented using the Bioruptor UCD-300 sonication
400 device (Diagenode, Denville, NJ, USA). Libraries were prepared using the Kapa Library Preparation Kit
401 KR0453-v2.13 (Kapa Biosystems, Wilmington, MA, USA) following the manufacturer's instructions with
402 five minor modifications. First, we used half volume reactions. Second, subsequent to end repair, we
403 added Sera-Mag Speedbeads (Thermo-Scientific, Waltham, MA, USA; prepared according to (Glenn et al.
404 2016)) at a ratio of 2.86:1 for end repair cleanup. Third, we ligated universal iTru y-yoke adapters (Glenn
405 et al. 2016) onto the genomic DNA. Fourth, following adapter ligation, we performed one post-ligation
406 cleanup followed by Dual-SPRI size selection using 55 µL of speedbead buffer (22.5mM PEG, 1M NaCl)
407 and 25 µL of Speedbeads. Finally, we performed a PCR at 95 °C for 45 sec, then 14 cycles of 98 °C for 30
408 sec, 60 °C for 30 sec, 72 °C for 30sec, then 72 °C for a 5 minute final extension and a 12 °C hold using
409 iTru5 and iTru7 primers to produce Illumina TruSeqHT compatible libraries (Glenn et al. 2016).

410 Libraries were quantified on a Qubit 2.0 (Life Technologies) and 83 ng from each library was
411 added to create 5 pools of 6 or 7 libraries each. We then split the pools in two. One subsample was
412 enriched for UCE loci, the other was not. UCE loci in the enriched library pools were captured using
413 Tetrapods 5K version 1 baits from MYcroarray (Ann Arbor, MI, USA) following their MYbaits protocol v.
414 2.3.1 with overnight incubations (Faircloth et al. 2012). Enriched libraries were quantified with a Qubit
415 and pooled with other unrelated samples prior to sequencing on an Illumina HiSeq 3000 to produce
416 paired-end reads of ≤ 151 bases. The unenriched samples were sequenced on a separate run using a
417 single lane of Illumina HiSeq 2500. All samples were demultiplexed with Illumina's fastq2bcl software.
418 Reads were quality filtered by removing any potential adapter sequence and trimming read ends once

419 the average Phred quality over a four base window score dropped below 20 using the Fastx toolkit
420 (Gordon et al. 2010).

421 *Assembly, annotation, and phylogenetic analysis of the mitochondrial genome*

422 Raw reads from the unenriched libraries were used to generate mitochondrial genomes via
423 MitoBim (Hahn et al. 2013). This program used MIRA (Chevreux et al. 1999) to map reads to a *M.*
424 *brandtii* reference genome (Genbank accession number KT210199.1). Alternative methods of
425 mitochondrial genome assembly were used when MitoBim assembly failed. These taxa include *M.*
426 *albescens* (TK61766), *M. albescens* (TK 101723), *M. albescens* (RDS 7889), *M. fortidens*, M. *keeni*, *M.*
427 *melanorhinus*, *M. nigricans* (QCAZ 9601), *M. septentrionalis*, *M. simus*, *M. velifer*, and *M. volans*. For
428 these samples, we first identified reads that were mitochondrial in origin using BLAST searches against
429 the *M. brandtii* mitochondrial genome (KT210199.1). Those reads were assembled using Trinity v2.2.0
430 with the '–single' option to treat reads as unpaired. For taxa where we used NCBI genome assemblies to
431 recover UCE loci *in silico* mitochondrial genomes from genbank were used to in the mitochondrial
432 analyses GenBank as follows: *M. brandti*i (KT210199.1), *E. fuscus* (KF111725.1), *M. lucifugus*
433 (KP273591.1), and *M. davidii* (KM233172.1).

434 Once assembled, each mitogenome was annotated via MITOS (Bernt et al. 2013). Annotated
435 genes were manually validated via BLAST to confirm sequence identity and length. Protein coding genes
436 were checked for stop codons using EMBOSS's transeq program (Rice et al. 2000). When a stop codon
437 was found, we used the raw reads to verify the sequence. We used BWA v0.7.12 (Li, Heng et al. 2009) to
438 align the reads to the Mitobim assembled mitogenome to verify base calls from Mitobim. The protein
439 coding rRNA and tRNA genes from each assembly were aligned using MUSCLE and concatenated into
440 three different alignments containing only protein coding genes, only rRNA and tRNA genes, or all
441 protein coding and RNA genes. A fourth alignment of all protein coding genes was translated to amino
442 acids and concatenated into a single alignment.

443 Several different partitioning schemes were examined for each of the mitochondrial alignments.
444 Alignments were either partitioned by gene, by codon, or by gene type (rRNA and tRNA vs. protein
445 coding). Genes were partitioned individually except in the instances where two genes overlapped. These
446 regions were partitioned separately from the individual genes resulting in three partitions for the two
447 genes: a partition for gene A, a partition for gene B, and a partition for the overlapping nucleotides of
448 gene A and B.

449 *Assembly, and phylogenetic analysis of nuclear UCEs*

450 Quality filtered raw sequence reads from the UCE-enriched libraries were assembled into
451 contigs using the Trinity assembler (Grabherr et al. 2011) with a minimum kmer coverage of 2. We used
452 Phyluce to identify those assembled contigs that were UCE loci. We also harvested UCE loci from
453 *Eptesicus fuscus* (GCA_000308155.1), *Myotis brandtii* (GCA_000412655.1), *M. davidii*
454 (GCA_000327345.1), and *M. lucifugus* (GCF_000147115.1) genome assemblies using the Phyluce
455 package (Faircloth 2016). Once extracted from Trinity and genome assemblies, we aligned all UCE loci
456 MAFFT (Katoh et al. 2002) and trimmed the aligned data with gBlocks (Castresana 2000). Repetitive
457 sequences (i. e. transposable elements) in each alignment were identified with RepeatMasker and
458 trimmed where found.

459 Each alignment was analyzed using three different partitioning schemes. Unpartitioned
460 alignments were simply concatenated UCE loci treated as a single unit. These alignments are referred to
461 herein as "unpartitioned". Fully partitioned alignments were concatenated alignments mitochondrial
462 genes that were partitioned by locus. These alignments are referred to herein as "locus partitioned".
463 Finally, PartitionFinder v1.1.1 (Lanfear et al. 2012) was used to combine individual loci into an optimal
464 partitioning scheme. The combined partitioning schemes for each alignment were identified with
465 PartitionFinder v1.1.1 (Lanfear et al. 2012). Rather than searching for best-fit substitution models for
466 each locus or partition, the GTR+Γ model of sequence evolution was assigned to all loci (Darriba et al.
467 2015) except in the case of amino acid alignments where the MtMam model was used. Initial trees for
468 PartitionFinder were generated using RAxML v7.4.1 (Stamatakis 2006) with linked branch lengths.
469 Partitioning schemes were heuristically searched using the hcluster algorithm. Partitioning schemes
470 were chosen using the Bayeisan information criterion.

471 Finally, each alignment and partitioning scheme was analyzed using Bayesian inference and
472 maximum likelihood phylogenetic methods. Bayesian phylogenies were generated with the MPI version
473 of ExaBayes (v1.4.1) using 4 independent runs of 4 chains each. ExaBayes runs were terminated after 10
474 million generations only if the average standard deviation of split frequencies was less than 0.01. The
475 first 25% of samples were discarded after which every 1,000th generation was sampled. Proper sampling,
476 post burn-in was inspected via Tracer v1.6. (Rambaut et al. 2014) and effective sample sizes greater than
477 200 were considered acceptable. Posterior probability values greater than 95% were considered to be
478 significant. RaxML (v8.1.3) was used to estimate and score the maximum likelihood phylogeny with the
479 rapid bootstrapping option and 10,000 bootstrap replicates. We define strongly supported bipartitions
480 as those present in 95-100% of bootstrap replicates and moderately supported bipartitions are present
481 in 85-95% of bipartitions (Wiens et al. 2008). All mitochondrial analyses are described in Table 3.

482 *Alignment types.* – Different combinations of UCE loci were used to create unique matrices
483 based on 1) locus distribution, 2) locus length, or 3) random locus sampling. The first set of alignments
484 (locus distribution) was determined by the number of taxa represented in the UCE alignments
485 (phyluce_align_get_only_loci_with_min_taxa; Faircloth 2016), or degree of completeness. Matrices
486 were constructed using loci which were present in 100% (number of specimens = 37), 95% (n = 35), 85%
487 (n = 31), 75% (n = 27), 65% (n = 24), 55% (n = 20), 45% (n = 16), 35% (n = 12), 25% (n = 9), and 15% (n = 5)
488 of specimens examined. These 10 groups were non-exclusive, so a locus that was assembled in all
489 specimens (100% complete) would also be included with loci present in only 55% of specimens. On the
490 other hand, a locus found in only 55% of specimens would not be included in the 100% complete data
491 set. Each set of UCE alignments was concatenated using phyluce_align_format_nexus_files_for_raxml
492 and a nexus character block was created using the phyluce_align_format_nexus_files_for_raxml –
493 charsets option. These datasets then served as the basis for downstream phylogenetic analyses. For
494 example, when a partitioning methodology (discussed below) was tested, it was performed for each of
495 the 100%, 95%, 85%, etc. alignments. In addition to partitioning schemes, the effect of missing data was
496 examined using Bayesian and maximum likelihood methods.
497 The second alignment criteria combined UCE loci of similar sizes. Pervious coalescent analyses of
498 UCE data showed that sub-sampling the most informative loci can result in different topologies
499 (Meiklejohn et al. 2016). Rather than using coalescent based analyses we used concatenation of UCE loci
500 to identify different topologies based on length. Under these assumptions, UCE loci were sorted into ten
501 groups based on their length and the predicted correlation between length and number of informative
502 characters was confirmed (Supplemental Figure 1). UCE loci in the same size cohort were combined into
503 a single alignment, partitioned by locus, and analyzed with RAxML using the methods described below.
504 The final set of alignments was generated by random sampling of UCE loci. In large phylogenetic
505 analyses, systematic error can result in highly supported, but incorrect topologies due to compounding
506 of non-phylogenetic signal (Rodríguez-Ezpeleta et al. 2007). By randomly reducing the dataset and
507 replicating the maximum likelihood analyses, we can reduce the potential effects of compounding error.
508 Roughly 10% of the dataset, 365 loci, were randomly sampled, concatenated, and partitioned by locus to
509 create 100 new alignments, which were then analyzed with RAxML using the methods described below.
510 *Partitioning strategies.* –Alignments were analyzed using three different partitioning schemes –
511 single, locus, and combined- similar to the mitochondrial partitioning schemes described above.
512 Unpartitioned alignments were simply concatenated UCE loci treated as a single genetic unit. Rather
513 than searching for best-fit substitution models for each UCE locus or partition, the GTR+Γ model of

514 sequence evolution was assigned to all loci (Darriba et al. 2015). Initial trees for PartitionFinder were
515 generated using RAxML v7.4.1 (Stamatakis 2006) with linked branch lengths. Partitioning schemes were
516 heuristically searched using the hcluster algorithm and the best scheme was chosen using the Bayesian
517 information criterion.

518 *Inference methods.* –Phylogenetic trees were generated with three different phylogenetic
519 inference methods across five different inference implementations including concatenation and
520 summary tree methods.

521 Maximum likelihood trees were inferred for each alignment and partitioning combination using
522 RAxML v8.1.3 (Aberer et al. 2014). The best scoring (lowest -lnL) tree from each dataset was identified
523 from 100 random starting trees and bootstrapped 100 times using the GTR+Γ in both cases. The
524 autoMRE function in RAxML v8.1.3 was used to determine the need for additional bootstrap replicates
525 beyond the initial 100 (Pattengale et al. 2009). A stopping criterion was set *a priori* if the weighted
526 Robinson-Foulds distance was less than 5% in 95% of random permutations of computed bootstrap
527 replicates (Pattengale et al. 2009). If necessary, an additional 100 bootstrap replicates were computed
528 until the convergence stopping criteria were met. Finally, bipartition frequencies of bootstrap replicates
529 were drawn onto the best scoring tree from the initial RAxML searches for each of the respective data
530 sets. Alignments based on UCE length or randomly sampled were analyzed using slightly different
531 methods. In both cases UCE loci were partitioned individually and nodal support was calculated using
532 100 bootstrap replicates using the RAxML fast-bootstrapping option. For all maximum likelihood
533 analyses, we define strongly supported bipartitions as those present in 95-100% of bootstrap replicates
534 and moderately supported bipartitions are present in 85-95% of bipartitions (Wiens et al. 2008).

535 Bayesian analyses were conducted using ExaBayes v1.4.1 (Aberer et al. 2014). For all Bayesian
536 analyses four independent runs of four chains each were run in parallel for a minimum of one million
537 generations sampling every thousandth generation and applying a GTR+Γ substitution model for each
538 partition. After one million generations, analyses continued until the standard deviation of the split
539 frequency between chains was less than 0.01. The "-M 3" option was used to reduce the memory
540 footprint of all ExaBayes runs. Proper sampling, post burn-in, was inspected via Tracer v1.6. (Rambaut et
541 al. 2014). Effective sample sizes greater than 200 were considered acceptable. Posterior probability
542 values greater than 95% were considered significant. An extended majority rule consensus tree was
543 created from all trees after the first 25% of trees were discarded using TreeAnnotator v1.7.0 (Rambaut
544 et al. 2013) and parameter estimates across all runs were calculated with Tracer v1.6 (Rambaut et al.
545 2014).

546 Species trees were calculated from gene trees for individual UCE loci recovered in five or more
547 taxa using the GTR+Γ substitution model and fast bootstrapping (-f a) option in RAxML and 1,000
548 bootstrap replicates. In general, gene trees were classified based on the degree of completeness (i.e.
549 number of taxa represented) similar to the way we treated individuals as described above.

550 Species trees were estimated and bootstrapped using three different programs. ASTRAL-II v4.10
551 (Mirarab et al. 2015) was used to build a summary tree. Support values for bipartitions in the tree were
552 generated from 100 bootstrap replicates using site as well as site and locus resampling (Seo 2008).
553 Species trees were estimated from ASTRID v1.4 (Vachaspati et al. 2015) using bionj and bootstrapped
554 for 100 replicates. SVDquartets (Chifman et al. 2014), as implemented in PAUP v4.0a150 (Swofford
555 2003), was used to estimate a species trees from a random subset of 200,000 quartets and 1,000
556 bootstrap replicates.

557 UCE loci are relatively short markers with few informative characters from which to build gene
558 trees. Errors in gene tree estimation may reduce the accuracy of summary methods and phylogenetic
559 inference (Liu et al. 2009, Leaché et al. 2011, DeGiorgio et al. 2014, Mirarab et al. 2016). We used
560 weighted and unweighted statistical binning to combine gene into compatible supergenes, increasing
561 the number of informative informative characters per "locus" and reducing the phylogenetic error
562 (Mirarab et al. 2014, Bayzid et al. 2015). The gene trees used for the summary tree methods described
563 above were used rather than re-estimating trees. Bifurcations supported by more than 50% of the
564 bootstrap replicates were retained for each gene tree. Alignments from compatible trees were
565 concatenated into a single supergene alignment. Trees for supergenes were estimated using RAxML. The
566 best trees for each supergene, as defined by log likelihood score, were retained from 500 searches.
567 Bipartition support was estimated from 500 bootstrap replicates. For all analyses, the GTR+Γ model of
568 substitution was used and each gene in the supergene alignment was partitioned separately. The
569 resulting supertrees were then used for species tree estimation using ASTRAL-II. For the unweighted
570 analysis, all supertrees were included in the pool of trees. For the weighted analysis, supertrees were
571 weighted according to the number of genes combined in the supergene alignment. For example, if a
572 supergene was a composite of six genes, the supertree was present 6 times compared to a composite of
573 five genes which would be represented only five times. Support for the weighted and unweighted
574 species trees was estimated by site and site and locus re-sampling (Seo 2008) for 100 bootstrap
575 replicates in ASTRAL-II.

576 *Topological comparisons*–

577 Trees recovered from all analyses were compared to each other in order to quantify the
578 differences between topologies. Branch lengths have different meanings based on the type of analysis.
579 For example, ASTRAL-II branch lengths are representative of coalescent units. ASTRID doesn't even
580 calculate branch lengths. For accurate tree comparisons, branch lengths were stripped from all trees.
581 Pairwise unweighted Robinson-Foulds distances were calculated among all trees. Robinson-Foulds
582 distances were transformed into two dimensions using the stochastic CCA algorithm for nonlinear
583 dimension reduction in TreeScaper v1.09 (Huang, Wen et al. 2016). Coordinates were then visualized in
584 R using hexagonal binning in the hexbin library v1.27.1 (Lewin-Koh 2011). Nuclear and mitochondrial
585 50% majority rule consensus trees were generated with PAUP v4.0a150 (Swofford 2003).
586
587 **Acknowledgments:**
588 We would like to thank the following museums, collection managers, and collaborators for the
589 tissue loans necessary to complete this work: Joseph Cook (Museum of Southwestern Biology), Museum
590 of Vertebrate Zoology, Manuel Ruedi (Natural History Museum of Geneva), Santiago Burneo (Pontificia
591 Universidad Catolica del Ecuador Museo de Zoologia), Heath Garner, Robert Bradley and Caleb Phillips
592 (Texas Tech University Natural Science Research Laboratory), Link Olson (University of Alaska Museum
593 of the North), Cody Thompson and Priscilla Tucker (University of Michigan Museum of Zoology). In
594 addition, we would like to thank the Texas Tech HPCC (http://www.depts.ttu.edu/hpcc/) for providing
595 the computational resources necessary to complete this project. This work was supported by the
596 National Science Foundation, DEB-1355176. Additional support was provided by College of Arts and
597 Sciences at Texas Tech University. All sequence data is available at NCBI's Short Read Archive
598 (SRP095250). UCE contig assemblies are available at (PENDING ACCESSION NUMBER). Supplemental files
599 include: a nexus file containing all estimated species trees (supFile-all_trees_2017-06-07.nexus.txt), and
600 tables listing each of the phylogenetic analyses. An archived file of individual UCE alignments in fasta
601 format (uceLociAlignments.tgz), and an archived file containing all individual UCE gene trees in newick
602 format (UceGeneTrees.tgz) are available through DRYAD (PENDING ACCESSION NUMBER).
603

604 **Figure and Table Captions**

605 **Figure 1.** Comparison of nuclear and mitochondrial phylogenetic trees of *Myotis*. The most common
606 mitochondrial (A) and nuclear (B) topologies. The mitochondrial topology arises from Bayesian and
607 maximum likelihood analysis of the amino acid sequences portioned based on the PartitonFinder
608 recommendations. The nuclear topology is from the 55% complete data matrix partitioned based on the
609 recommendations of PartitionFinder. For clarity, bootstrap values greater than 95 and clade probability
610 values greater than 0.95 have been omitted from the nuclear consensus tree. Majority-rule consensus
611 trees from 28 mitochondrial (C) and 294 nuclear (D) topologies. Values above the branches in the
612 consensus trees (C and D) are bipartition frequencies for that clade across all nuclear or mitochondrial
613 topologies. Conflicting tips between data types (consensus nuclear vs. consensus mitochondrial) are
614 indicated with red lines between the topologies. Biogeographic regions are color coded, as are
615 subgeneric classifications based on morphotypes, as defined by Findley (1972). Species with more than
616 one sample are designated with a superscript that is referenced in Table 1. Specimens derived from
617 whole genome alignments are designated with a superscript "G".

618 **Figure 2.** Comparison of mitochondrial and nuclear topologies. (A) All trees recovered from
619 mitochondrial and nuclear analyses were visualized in tree space using multidimensional scaling of
620 Robinson-Foulds distances. Nuclear trees (green outlines) were clustered separately from mitochondrial
621 trees (blue outlines). Robinson-Foulds distances between nuclear and mitochondrial trees (B), nuclear
622 vs. nuclear trees (C) and mitochondrial vs. mitochondrial trees (D) indicate the overall distinctions
623 between the nuclear and mitochondrial topologies.

624 **Table 1.** Specimens examined. Collection abbreviations: Museum of Southwestern Biology (MSB),
625 Museum of Vertebrate Zoology (MVZ), Natural History Museum of Geneva (MHNG), Pontificia
626 Universidad Catolica del Ecuador Museo de Zoologia (QCAZ), Texas Tech University Natural Science
627 Research Laboratory (TK), University of Alaska Museum of the North (UAM), University of Michigan
628 Museum of Zoology (UMMZ).

629 **Table 2.** General alignment information. For a subset of analyses a series of alignments were generated
630 based on the number of taxa per locus. Thirty-seven taxa were examined so an alignment with all 37
631 taxa was considered 100% complete. Parsimony-informative characters make up a small portion of the
632 total alignment. The number of partitions in the combined partitioning scheme was calculated with
633 PartitionFinder.

Sup Fig 1. Phylogenetic content of UCE loci based on length. The length of a UCE locus is correlated with the number of phylogenetically informative characters. UCE loci were sorted by length and ten bins of alignments were created so that the shortest loci were combined into one alignment, the next shortest set of loci were combined … etc. Parsimony informative characters made up a minor part of each alignment.

Sup File 1 - supFile-all_trees_2017-06-07.nexus.txt – Trees generated from all analyses in nexus format.

640 **Literature Cited**

641 Aberer A. J., Kobert K., Stamatakis A. 2014. ExaBayes: Massively parallel Bayesian tree inference for the
642 whole-genome era. Mol Biol Evol. 31:2553-2556.
643 Bayzid M. S., Mirarab S., Boussau B., Warnow T. 2015. Weighted statistical binning: Enabling statistically
644 consistent genome-scale phylogenetic analyses. PLoS ONE. 10:e0129183.
645 Bernt M., Donath A., Jühling F., Externbrink F., Florentz C., Fritzsch G., Pütz J., Middendorf M., Stadler P.
646 F. 2013. MITOS: Improved de novo metazoan mitochondrial genome annotation. Mol Phylogenet Evol.
647 69:313-319.
648 Bogdanowicz W., Piksa K., Tereba A. 2012. Hybridization hotspots at bat swarming sites. PLoS ONE.
649 7:e53334.
650 Boyles J. G., Storm J. J. 2007. The perils of picky eating: Dietary breadth is related to extinction risk in
651 insectivorous bats. PLOS ONE. 2:e672.
652 Caceres M. C., Barclay R. M. R. 2000. *Myotis septentrionalis*. Mammalian Species:1-4.
653 Carstens B. C., Dewey T. A. 2010. Species delimitation using a combined coalescent and information-
654 theoretic approach: An example from North American *Myotis* bats. Syst Biol. 59:400-414.
655 Castresana J. 2000. Selection of conserved blocks from multiple alignments for their use in phylogenetic
656 analysis. Mol Biol Evol. 17:540-552.
657 Chevreux B., Wetter T., Suhai S. 1999. Genome sequence assembly using trace signals and additional
658 sequence information. Proceedings of the German Conference on Bioinformatics (GCB).
659 Chifman J., Kubatko L. 2014. Quartet inference from SNP data under the coalescent model.
660 Bioinformatics. 30:3317-3324.
661 Darriba D., Posada D. 2015. The impact of partitioning on phylogenomic accuracy. bioRxiv.
662 https://doi.org/10.1101/023978.
663 DeGiorgio M., Degnan J. H. 2014. Robustness to divergence time underestimation when inferring species
664 trees from estimated gene trees. Syst Biol. 63:66-82.
665 Degnan J. H., Rosenberg N. A. 2009. Gene tree discordance, phylogenetic inference and the multispecies
666 coalescent. Trends Ecol Evol. 24:332-340.
667 Derti A., Roth F. P., Church G. M., Wu C. t. 2006. Mammalian ultraconserved elements are strongly
668 depleted among segmental duplications and copy number variants. Nat Genet. 38:1216-1220.
669 Douady C. J., Delsuc F., Boucher Y., Doolittle W. F., Douzery E. J. P. 2003. Comparison of Bayesian and
670 maximum likelihood bootstrap measures of phylogenetic reliability. Mol Biol Evol. 20:248-254.
671 Dzeverin I. 2008. The stasis and possible patterns of selection in evolution of a group of related species
672 from the bat genus *Myotis* (Chiroptera, Vespertilionidae). J Mamm Evol. 15:123-142.
673 Edwards S., Bensch S. 2009. Looking forwards or looking backwards in avian phylogeography? A
674 comment on Zink and Carrowclough 2008. Mol Ecol. 18:2930-2933.
675 Faircloth B. C. 2016. PHYLUCE is a software package for the analysis of conserved genomic loci.
676 Bioinformatics. 32:786-788.
677 Faircloth B. C., Branstetter M. G., White N. D., Brady S. G. 2015. Target enrichment of ultraconserved
678 elements from arthropods provides a genomic perspective on relationships among Hymenoptera. Mol
679 Ecol Resour. 15:489-501.
680 Faircloth B. C., McCormack J. E., Crawford N. G., Harvey M. G., Brumfield R. T., Glenn T. C. 2012.
681 Ultraconserved elements anchor thousands of genetic markers spanning multiple evolutionary
682 timescales. Syst. Biol. 61:717-726.
683 Findley J. S. 1972. Phenetic relationships among bats of the genus *Myotis*. Syst Biol. 21:31-52.
684 Fitch J. H., Shump K. A. 1979. *Myotis keenii*. Mammalian Species Archive. 121:1-3.
685 Glenn T. C., Nilsen R., Kieran T. J., Finger J. W., Pierson T. W., Bentley K. E., Hoffberg S., Louha S., Garcia-
686 De-Leon F. J., Angel del Rio Portilla M., Reed K., Anderson J. L., Meece J. K., Aggery S., Rekaya R., Alabady

687 M., Belanger M., Winker K., Faircloth B. C. 2016. Adapterama I: Universal stubs and primers for
688 thousands of dual-indexed Illumina libraries (iTru & iNext). bioRxiv. https://doi.org/10.1101/049114.
689 Good J. M., Vanderpool D., Keeble S., Bi K. 2015. Negligible nuclear introgression despite complete
690 mitochondrial capture between two species of chipmunks. Evolution. 69:1961-1972.
691 Gordon A., Hannon G. 2010. Fastx-toolkit. http://hannonlab.cshl.edu/fastx_toolkit.
692 Grabherr M. G., Haas B. J., Yassour M., Levin J. Z., Thompson D. A., Amit I., Adiconis X., Fan L.,
693 Raychowdhury R., Zeng Q., Chen Z., Mauceli E., Hacohen N., Gnirke A., Rhind N., di Palma F., Birren B.
694 W., Nusbaum C., Lindblad-Toh K., Friedman N., Regev A. 2011. Full-length transcriptome assembly from
695 RNA-Seq data without a reference genome. Nat Biotech. 29:644-652.
696 Green R. E., Braun E. L., Armstrong J., Earl D., Nguyen N., Hickey G., Vandewege M. W., St. John J. A.,
697 Capella-Gutiérrez S., Castoe T. A., Kern C., Fujita M. K., Opazo J. C., Jurka J., Kojima K. K., Caballero J.,
698 Hubley R. M., Smit A. F., Platt R. N., Lavoie C. A., Ramakodi M. P., Finger J. W., Suh A., Isberg S. R., Miles
699 L., Chong A. Y., Jaratlerdsiri W., Gongora J., Moran C., Iriarte A., McCormack J., Burgess S. C., Edwards S.
700 V., Lyons E., Williams C., Breen M., Howard J. T., Gresham C. R., Peterson D. G., Schmitz J., Pollock D. D.,
701 Haussler D., Triplett E. W., Zhang G., Irie N., Jarvis E. D., Brochu C. A., Schmidt C. J., McCarthy F. M.,
702 Faircloth B. C., Hoffmann F. G., Glenn T. C., Gabaldón T., Paten B., Ray D. A. 2014. Three crocodilian
703 genomes reveal ancestral patterns of evolution among archosaurs. Science. 346:1254449.
704 Hahn C., Bachmann L., Chevreux B. 2013. Reconstructing mitochondrial genomes directly from genomic
705 next-generation sequencing reads—a baiting and iterative mapping approach. Nucleic Acids Res.
706 41:e129.
707 Haynie M. L., Tsuchiya M. T. N., Ospina-Garcés S. M., Arroyo-Cabrales J., Medellín R. A., Polaco O. J.,
708 Maldonado J. E. 2016. Placement of the rediscovered *Myotis planiceps* (Chiroptera: Vespertilionidae)
709 within the *Myotis* phylogeny. J Mammal. 97:701-712.
710 Hedtke S. M., Townsend T. M., Hillis D. M. 2006. Resolution of phylogenetic conflict in large data sets by
711 increased taxon sampling. Syst Biol. 55:522-529.
712 Hollister N. 1909. Two new bats from the southwestern United States. publisher not identified.
713 Hosner P. A., Faircloth B. C., Glenn T. C., Braun E. L., Kimball R. T. 2016. Avoiding missing data biases in
714 phylogenomic inference: An empirical study in the landfowl (Aves: Galliformes). Mol Biol Evol. 33:1110-
715 1125.
716 Huang H., He Q., Kubatko L. S., Knowles L. L. 2010. Sources of error inherent in species-tree estimation:
717 Impact of mutational and coalescent effects on accuracy and implications for choosing among different
718 methods. Syst Biol. 59:573-583.
719 Huang W., Zhou G., Marchand M., Ash J. R., Morris D., Van Dooren P., Brown J. M., Gallivan K. A.,
720 Wilgenbusch J. C. 2016. TreeScaper: Visualizing and extracting phylogenetic signal from sets of trees.
721 Mol Biol Evol.
722 Hudson R. R., Coyne J. A., Huelsenbeck J. 2002. Mathematical consequences of the genealogical species
723 concept. Evolution. 56:1557-1565.
724 Kapusta A., Suh A., Feschotte C. 2017. Dynamics of genome size evolution in birds and mammals. Proc
725 Natl Acad Sci U S A. 114:E1460-E1469.
726 Katoh K., Misawa K., Kuma K. i., Miyata T. 2002. MAFFT: a novel method for rapid multiple sequence
727 alignment based on fast Fourier transform. Nucleic Acids Res. 30:3059-3066.
728 Lack J. B., Roehrs Z. P., Stanley C. E., Ruedi M., Van Den Bussche R. A. 2010. Molecular phylogenetics of
729 *Myotis* indicate familial-level divergence for the genus *Cistugo* (Chiroptera). J Mammal. 91:976-992.
730 Lanfear R., Calcott B., Ho S. Y. W., Guindon S. 2012. PartitionFinder: Combined selection of partitioning
731 schemes and substitution models for phylogenetic analyses. Mol Biol Evol. 29:1695-1701.
732 Larsen R. J., Knapp M. C., Genoways H. H., Khan F. A. A., Larsen P. A., Wilson D. E., Baker R. J. 2012.
733 Genetic diversity of neotropical *Myotis* (Chiroptera: Vespertilionidae) with an emphasis on South
734 American species. PLoS ONE. 7:e46578.

LaVal R. K. 1973. A revision of the Neotropical bats of the genus *Myotis*. Natural History Museum, Los Angeles County.
Leaché A. D., Rannala B. 2011. The accuracy of species tree estimation under simulation: A comparison of methods. Syst Biol. 60:126-137.
Leavitt D. H., Marion A. B., Hollingsworth B. D., Reeder T. W. 2017. Multilocus phylogeny of alligator lizards (Elgaria, Anguidae): Testing mtDNA introgression as the source of discordant molecular phylogenetic hypotheses. Mol Phylogenet Evol.
Lewin-Koh N. 2011. Hexagon binning: an overview. ftp://ftp.naist.jp/pub/lang/R/CRAN/web/packages/hexbin/vignettes/hexagon_binning.pdf.
Li G., Davis B. W., Eizirik E., Murphy W. J. 2016. Phylogenomic evidence for ancient hybridization in the genomes of living cats (Felidae). Genome Res. 26:1-11.
Li H., Durbin R. 2009. Fast and accurate short read alignment with Burrows–Wheeler transform. Bioinformatics. 25:1754-1760.
Liu L., Edwards S. V. 2015. Comment on "Statistical binning enables an accurate coalescent-based estimation of the avian tree". Science. 350:171-171.
Liu L., Yu L., Kubatko L., Pearl D. K., Edwards S. V. 2009. Coalescent methods for estimating phylogenetic trees. Mol Phylogenet Evol. 53:320-328.
Manning R. W., Jones J. K. 1989. *Myotis evotis*. Mammalian Species Archive. 329:1-5.
McCormack J. E., Harvey M. G., Faircloth B. C., Crawford N. G., Glenn T. C., Brumfield R. T. 2013. A Phylogeny of birds based on over 1,500 loci collected by target enrichment and high-throughput sequencing. PLoS ONE. 8:e54848.
McGee M. D., Faircloth B. C., Borstein S. R., Zheng J., Darrin Hulsey C., Wainwright P. C., Alfaro M. E. 2016. Replicated divergence in cichlid radiations mirrors a major vertebrate innovation. Proc R Soc Lond B Biol Sc. 283.
Meiklejohn K. A., Faircloth B. C., Glenn T. C., Kimball R. T., Braun E. L. 2016. Analysis of a rapid evolutionary radiation using Ultraconserved Elements: Evidence for a bias in some multispecies coalescent methods. Syst Biol. 65:612-627.
Miller Jr G. S., Allen G. 1928. The American bats of the genus *Myotis* and *Pixonyx*. Bulletin of the United States National Museum. 144:1-218.
Mirarab S., Bayzid M. S., Boussau B., Warnow T. 2014. Statistical binning enables an accurate coalescent-based estimation of the avian tree. Science. 346.
Mirarab S., Bayzid M. S., Warnow T. 2016. Evaluating summary methods for multilocus species tree estimation in the presence of incomplete lineage sorting. Syst Biol. 65:366-380.
Mirarab S., Warnow T. 2015. ASTRAL-II: Coalescent-based species tree estimation with many hundreds of taxa and thousands of genes. Bioinformatics. 31:i44-i52.
Morales A. E., Jackson N. D., Dewey T. A., O'Meara B. C., Carstens B. C. 2016. Speciation with gene flow in North American *Myotis* bats. Syst Biol.
O'Farrell M. J., Studier E. H. 1980. *Myotis thysanodes*. Mammalian Species. 137:1-5.
Pagan H. J. T., Smith J. D., Hubley R. M., Ray D. A. 2010. PiggyBac-ing on a Primate genome: Novel elements, recent activity and horizontal transfer. Genome Biol Evol. 2.
Pattengale N. D., Alipour M., Bininda-Emonds O. R. P., Moret B. M. E., Stamatakis A. 2009. How many bootstrap replicates are necessary? In: Batzoglou S editor. Research in Computational Molecular Biology: 13th Annual International Conference, RECOMB 2009, Tucson, AZ, USA, May 18-21, 2009. Proceedings. Berlin, Heidelberg, Springer Berlin Heidelberg, p. 184-200.
Piaggio A. J., Valdez E. W., Bogan M. A., Spicer G. S. 2002. Systematics of *Myotis occultus* (Chiroptera: Vespertilionidae) inferred from sequences of two mitochondrial genes. J Mammal. 83:386-395.
Platt R. N., Mangum S. F., Ray D. A. 2016. Pinpointing the vesper bat transposon revolution using the Miniopterus natalensis genome. Mob DNA. 7:12.

783 Platt R. N., Vandewege M. W., Kern C., Schmidt C. J., Hoffmann F. G., Ray D. A. 2014. Large numbers of
784 novel miRNAs originate from DNA transposons and are coincident with a large species radiation in bats.
785 Mol Biol Evol. 31:1536-1545.
786 Platt R. N., Zhang Y., Witherspoon D. J., Xing J., Suh A., Keith M. S., Jorde L. B., Stevens R. D., Ray D. A.
787 2015. Targeted Capture of Phylogenetically Informative Ves SINE Insertions in Genus Myotis. Genome
788 Biol Evol. 7:1664-1675.
789 Pritham E. J., Feschotte C. 2007. Massive amplification of rolling-circle transposons in the lineage of the
790 bat *Myotis* lucifugus. Proc Natl Acad Sci U S A. 104:1895-1900.
791 Puechmaille S. J., Allegrini B., Boston E. S. M., Dubourg-Savage M.-J., Evin A., Knochel A., Le Bris Y., Lecoq
792 V., Lemaire M., Rist D., Teeling E. C. 2012. Genetic analyses reveal further cryptic lineages within the
793 *Myotis nattereri* species complex. Mammalian Biology. 77:224-228.
794 Rambaut A., Drummond A. 2013. TreeAnnotator v1. 7.0. http://beast.bio.ed.ac.uk.
795 Rambaut A., Suchard M., Xie D., Drummond A. 2014. Tracer v1.6. http://beast.bio.ed.ac.uk.
796 Ray D. A., Feschotte C., Pagan H. J. T., Smith J. D., Pritham E. J., Arensburger P., Atkinson P. W., Craig N.
797 L. 2008. Multiple waves of recent DNA transposon activity in the bat, *Myotis lucifugus*. Genome Res.
798 18:717-728.
799 Ray D. A., Pagan H. J. T., Thompson M. L., Stevens R. D. 2007. Bats with hATs: Evidence for recent DNA
800 transposon activity in genus *Myotis*. Mol Biol Evol. 24:632-639.
801 Rice P., Longden I., Bleasby A. 2000. EMBOSS: the European molecular biology open software suite.
802 Elsevier Current Trends.
803 Rodríguez-Ezpeleta N., Brinkmann H., Roure B., Lartillot N., Lang B. F., Philippe H. 2007. Detecting and
804 overcoming systematic errors in genome-scale phylogenies. Syst Biol. 56:389-399.
805 Roehrs Z. P., Lack J. B., Van Den Bussche R. A. 2010. Tribal phylogenetic relationships within
806 Vespertilioninae (Chiroptera: Vespertilionidae) based on mitochondrial and nuclear sequence data. J
807 Mammal. 91:1073-1092.
808 Ruedi M., Mayer F. 2001. Molecular systematics of bats of the genus *Myotis* (Vespertilionidae) suggests
809 deterministic ecomorphological convergences. Mol Phylogenet Evol. 21:436-448.
810 Ruedi M., Stadelmann B., Gager Y., Douzery E. J. P., Francis C. M., Lin L.-K., Guillén-Servent A., Cibois A.
811 2013. Molecular phylogenetic reconstructions identify East Asia as the cradle for the evolution of the
812 cosmopolitan genus *Myotis* (Mammalia, Chiroptera). Mol Phylogenet Evol. 69:437-449.
813 Seo T.-K. 2008. Calculating bootstrap probabilities of phylogeny using multilocus sequence data. Mol Biol
814 Evol. 25:960-971.
815 Simões B. F., Rebelo H., Lopes R. J., Alves P. C., Harris D. J. 2007. Patterns of genetic diversity within and
816 between *Myotis d. daubentonii* and *M. d. nathalinae* derived from cytochrome *b* mtDNA sequence data.
817 Acta Chiropt. 9:379-389.
818 Sota T. 2002. Radiation and reticulation: extensive introgressive hybridization in the carabid beetles
819 *Ohomopterus* inferred from mitochondrial gene genealogy. Population Ecology. 44:0145-0156.
820 Stadelmann B., Lin L. K., Kunz T. H., Ruedi M. 2007. Molecular phylogeny of New World *Myotis*
821 (Chiroptera, Vespertilionidae) inferred from mitochondrial and nuclear DNA genes. Mol Phylogenet Evol.
822 43:32-48.
823 Stamatakis A. 2006. RAxML-VI-HPC: maximum likelihood-based phylogenetic analyses with thousands of
824 taxa and mixed models. Bioinformatics. 22:2688-2690.
825 Swofford D. L. 2003. PAUP*. Phylogenetic analysis using parsimony (* and other methods). Version 4.
826 Thomas J., Sorourian M., Ray D., Baker R. J., Pritham E. J. 2011. The limited distribution of Helitrons to
827 vesper bats supports horizontal transfer. Gene. 474:52-58.
828 Vachaspati P., Warnow T. 2015. ASTRID: Accurate Species TRees from Internode Distances. BMC
829 Genomics. 16:S3.

Valdez E. W., Choate J. R., Bogan M. A., Yates T. L. 1999. Taxonomic status of *Myotis occultus*. J Mammal. 80:545-552.

Warner R. M. 1982. *Myotis auriculus*. Mammalian Species. 191:1-3.

Wiens J. J., Kuczynski C. A., Smith S. A., Mulcahy D. G., Sites J. J. W., Townsend T. M., Reeder T. W. 2008. Branch lengths, support, and congruence: Testing the phylogenomic approach with 20 nuclear loci in snakes. Syst Biol. 57:420-431.

Willis S. C., Farias I. P., Ortí G. 2014. Testing mitochondrial capture and deep coalescence in Amazonian cichlid fishes (Cichlidae: *Cichla*). Evolution. 68:256-268.

Table 1 - Specimens Examined

Species	Name herein	Museum identification num.	Num. UCE Loci	UCE contig accession	Mitochondrial genome accession
Eptesicus fuscus	*fuscus* [G]	GCA_000308155.1	2,467	Pending	KF111725.1
Eptesicus fuscus	*fuscus*	TK 178736	2,849	Pending	MF143474
Myotis albescens	*albescens* [1]	RDS 7889	2,764	Pending	MF143471
Myotis albescens	*albescens* [2]	QCAZ 9157	1,185	Pending	MF143497
Myotis albescens	*albescens* [3]	TK 61766	2,872	Pending	MF143470
Myotis ater	*ater*	M4430	2,774	Pending	MF143493
Myotis auriculus	*auriculus*	MSB 40883	2,229	Pending	MF143486
Myotis brandtii	*brandtii* [G]	GCA_000412655.1	2,446	Pending	KT210199.1
Myotis californicus	*californicus*	UMMZ 175828	2,948	Pending	MF143469
Myotis davidii	*davidii* [G]	GCA_000327345.1	2,450	Pending	KM233172.1
Myotis diminutus	*diminutus*	QCAZ 9168	3,078	Pending	MF143481
Myotis dominicensis	*dominicensis*	TK 15624	2,576	Pending	MF143467
Myotis evotis	*evotis*	MSB 47323	2,586	Pending	MF143468
Myotis fortidens	*fortidens*	MSB 54941	2,791	Pending	MF143483
Myotis horsfieldii	*horsfieldii*	MHNG 1926.039	3,017	Pending	MF143494
Myotis keaysi	*keaysi*	TK 13525	3,195	Pending	MF143477
Myotis keenii	*keenii*	UAM 113849	2,723	Pending	MF143472
Myotis leibii	*leibii*	TK 24872	3,119	Pending	MF143488
Myotis levis	*levis*	RDS 7781	2,538	Pending	MF143482
Myotis lucifugus	*lucifugus* [G]	GCA_000147115.1	2,429	Pending	KP273591.1
Myotis lucifugus	*lucifugus*	MSB 46679	2,736	Pending	MF143491
Myotis melanorhinus	*melanorhinus*	TK 193888	3,177	Pending	MF143489
Myotis nigricans	*nigricans* [1]	QCAZ 9601	2,854	Pending	MF143495
Myotis nigricans	*nigricans* [2]	TK 194145	3,159	Pending	MF143484
Myotis nyctor	*nyctor*	TK 151413	856	Pending	MF143498
Myotis occultus	*occultus*	MSB 121995	2,957	Pending	MF143490
Myotis oxyotus	*oxyotus*	UMMZ RCO1013	3,106	Pending	MF143479
Myotis riparius	*riparius* [1]	TK 22688	2,924	Pending	MF143473
Myotis riparius	*riparius* [2]	TK 101723	2,990	Pending	MF143475
Myotis riparius	*riparius* [3]	TK 145199	2,890	Pending	MF143480
Myotis ruber	*ruber*	MVZ 185692	2,757	Pending	MF143478
Myotis septentrionalis	*septentrionalis*	TK 194420	2,916	Pending	MF143487
Myotis thysanodes	*thysanodes*	07LEP	2,821	Pending	MF143492
Myotis velifer	*velifer*	MSB 70877	2,704	Pending	MF143499
Myotis vivesi	*vivesi*	MSB 42658	2,469	Pending	MF143476
Myotis volans	*volans*	MSB 40886	2,819	Pending	MF143496
Myotis yumanensis	*yumanensis*	TK 194144	2,589	Pending	MF143485

Collection abbreviations: Museum of Southwestern Biology (MSB), Museum of Vertebrate Zoology (MVZ), Natural History Museum of Geneva (MHNG), Pontificia Universidad Catolica del Ecuador Museo de Zoologia (QCAZ), Texas Tech University Natural Science Research Laboratory (TK), University of Alaska Museum of the North (UAM), University of Michigan Museum of Zoology (UMMZ). Samples beginning with "GCA_" represent genome assemblies available through NCBI.

Table 2. Character information

Min. num. of taxa	Percent of taxa per locus	Number of Loci	Parsimony-informative characters	Variable uninformative	Alignment length	Optimum Partitions
5	15	3,648	38,718	62,588	1,377,262	31
9	25	3,379	37,894	57,672	1,260,248	37
12	35	3,232	37,259	56,453	1,227,093	34
16	45	3,064	36,539	54,782	1,187,492	31
20	55	2,890	35,284	53,200	1,144,471	27
24	65	2,668	34,373	51,148	1,091,620	27
27	75	2,481	33,031	48,732	1,041,099	20
31	85	2,034	29,179	41,711	903,903	16
35	95	1,193	18,288	24,189	575,321	15
37	100	212	3,480	4,778	112,125	6
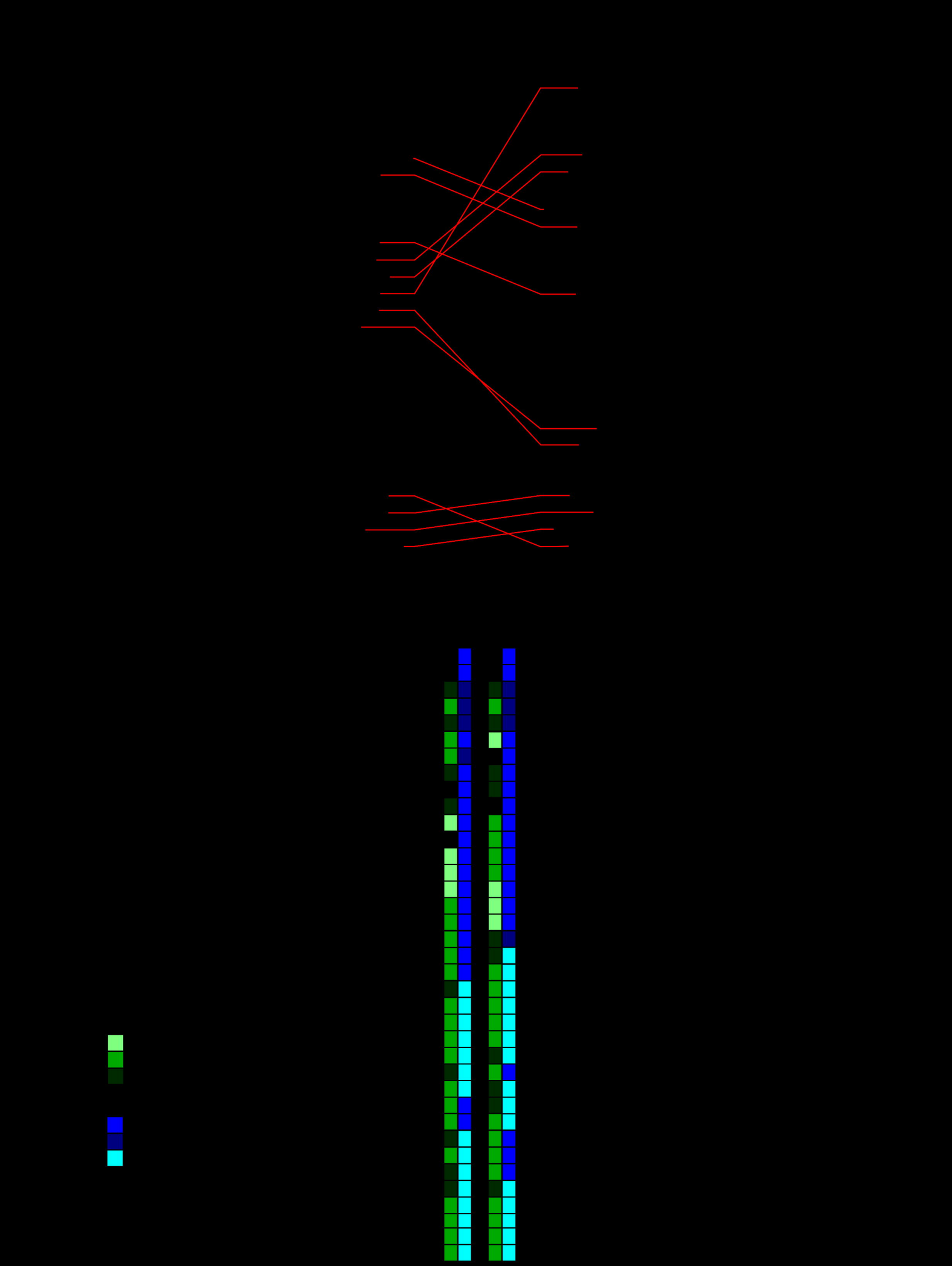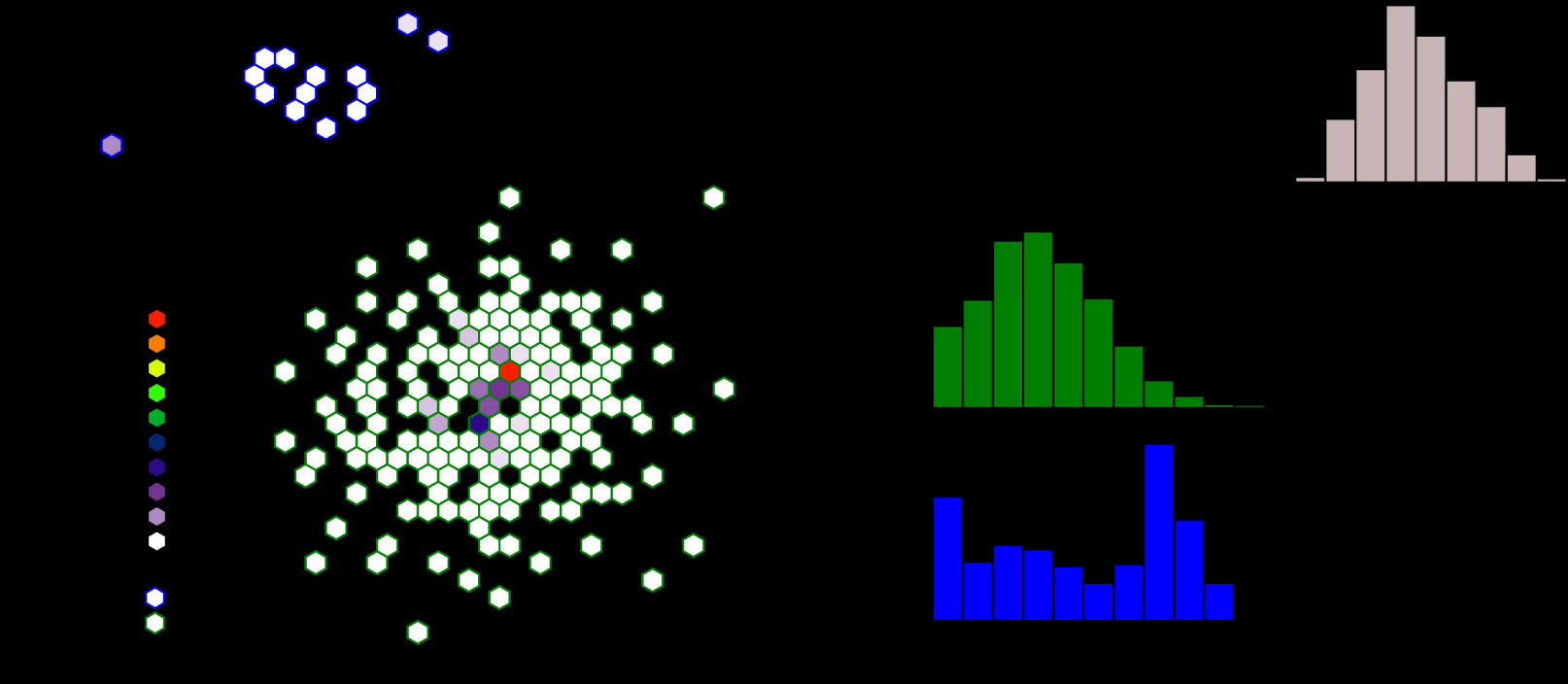
General alignment information. For a subset of analyses a series of alignments were generated based on the number of taxa per locus. Thirty-seven taxa were examined so an alignment with all 37 taxa was considered 100% complete. Parsimony-informative characters make up a small portion of the total alignment. The optimum partitioning scheme was calculated with PartitionFinder.